Hydrodynamic modeling of femtosecond laser ablation of metals in vacuum and in liquid

Mikhail E. Povarnitsyn & Tatiana E. Itina

Applied Physics A
Materials Science & Processing

ISSN 0947-8396

Appl. Phys. A
DOI 10.1007/s00339-014-8319-1

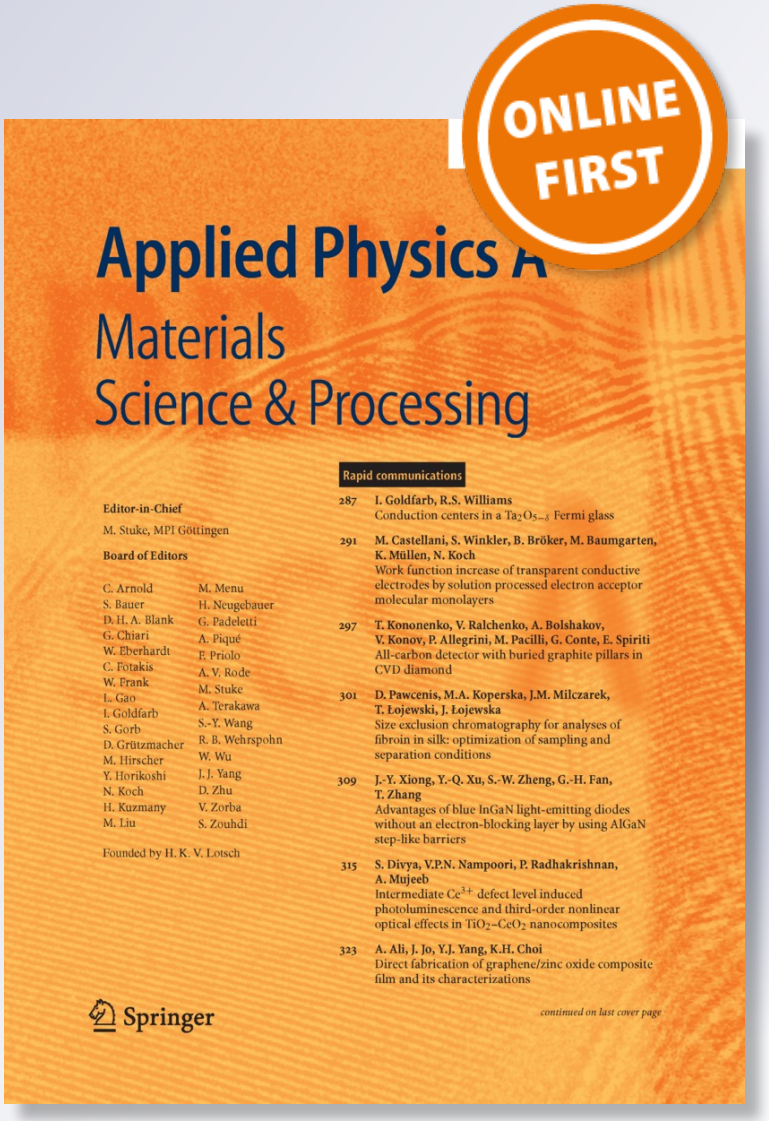

Springer

Appl. Phys. A
DOI 10.1007/s00339-014-8319-1

Applied Physics A
Materials Science & Processing

Hydrodynamic modeling of femtosecond laser ablation of metals in vacuum and in liquid

Mikhail E. Povarnitsyn · Tatiana E. Itina

Received: 4 November 2013 / Accepted: 11 February 2014

Abstract We numerically examine the mechanisms involved in nanoparticle formation by laser ablation of metallic targets in vacuum and in liquid. We consider the very early ablation stage providing initial conditions for much longer plume expansion processes. In the case of ultrashort laser ablation, the initial population of primary nanoparticles is formed at this stage. When a liquid is present, the dynamics of the laser plume expansion differs from that in vacuum. Low compressibility of the ambient liquid results in strong confinement conditions. As a result, ablation threshold rises drastically, the ablated material is compressed, part of it becomes supersaturated and the backscattered material additionally heats the target. The extension of a molten layer leads to the additional ablation at a later stage also favoring nanoparticle formation. The obtained results thus explain recent experimental findings and help to predict the role of the experimental parameters. The performed analysis indicates ways of a control over nanoparticle synthesis.

1 Introduction

Laser ablation (LA) is a simple and versatile technique for synthesis of nanoparticles and has found many applications in photonics, electronics and medicine [1, 2]. The major advantages of this method are in its nonchemical character and in the possibility of a control over particle size. These advantages make LA a unique tool for nanoparticle (NP) synthesis [3]. During the last decade, numerous experiments have been performed, clearly demonstrating that an interaction of a short (several nanoseconds or shorter) laser pulse with a solid target leads to the formation of NPs. It was shown that in the case of femtosecond LA, laser energy deposition induces an explosive ejection of a mixture of clusters and atoms [4, 5, 6, 7, 8, 9] rather than an equilibrium surface evaporation. Previously, classical continuous hydrodynamics was used to model laser plume expansion and Zel'dovich–Raizer model was employed to study condensation process in laser plumes [10, 11, 12, 13]. In addition, LA in liquids is known to be a particularly promising fabrication method of colloidal NPs [14, 15, 16, 17] with both small average size and dispersion. In this case, laser interactions take place under a strong confinement that modifies ablation plume parameters [18, 19].

Despite a large number of the experimental results obtained for LA, there are still many puzzling issues in the physical and chemical mechanisms of NP formation. In fact, it is unclear how and when NPs appear in the presence of liquid. Are they formed as a result of nucleation? Are they ejected from the target? Or, are they formed at a longer delay due to plume–liquid mixing? In particular, the presented calculations allow one to explain the experimental fact that typically, ablation threshold is larger in liquid than in vacuum [20]. Then, the enhanced NP production in the presence of liquid [14, 21] is also addressed. Furthermore, different mechanisms of NP formation indicated by the modeling explain the appearance of different populations of NPs [22, 23].

In this paper, we present numerical results obtained for femtosecond LA of metal targets (Al) in vacuum and in

M. E. Povarnitsyn (✉)
Joint Institute for High Temperatures, RAS, Moscow 125412, Russia
e-mail: povar@ihed.ras.ru

T. E. Itina
Hubert Curien Laboratory, CNRS/Lyon University, 42000 Saint-Étienne, France
e-mail: tatiana.itina@univ-st-etianne.fr

Published online: 27 February 2014

liquid (water). Using hydrodynamic numerical method [24], we investigate conditions that trigger the mechanisms of NP formation. We focus our attention on the role of the background environment. As a result, we demonstrate how the background medium affects the plume dynamics leading to material backscattering, additional target heating and providing additional roots for NP production.

2 Numerical approach

To examine the initial stage of the target response upon femtosecond laser irradiation in water, we apply the previously developed 1D Lagrangian two-temperature multi-material hydrodynamic model [25]. The laser energy absorption by the conduction band electrons in the target is taken into account by calculation of a source term based on a time and space-dependent profile of the complex dielectric function using a transfer matrix method [26]. Electron thermal conductivity is modeled by solving the heat diffusion equation in Fourier form. The electron–ion coupling factor is calculated using the model described in [27]. To complete the model, we use a two-temperature multi-phase equation of state for aluminum with Thomas–Fermi expression for the thermal contribution of electrons. Here, water is considered as a compressible but transparent and nonconductive material [25].

3 Results and discussion

Calculations are performed for LA of aluminum bulk target by $\tau_L = 100$ fs and $\lambda_L = 800$ nm normally incident laser pulses with fluences from 0.5 to 10 J/cm^2. The pulse has a Gaussian profile with the maximum at $t = 0$ ps so that the incident intensity is given by expression $I(t) = I_L \exp[-\ln(16)t^2/\tau_L^2]$. Initially, at $t = -0.5$ ps, the

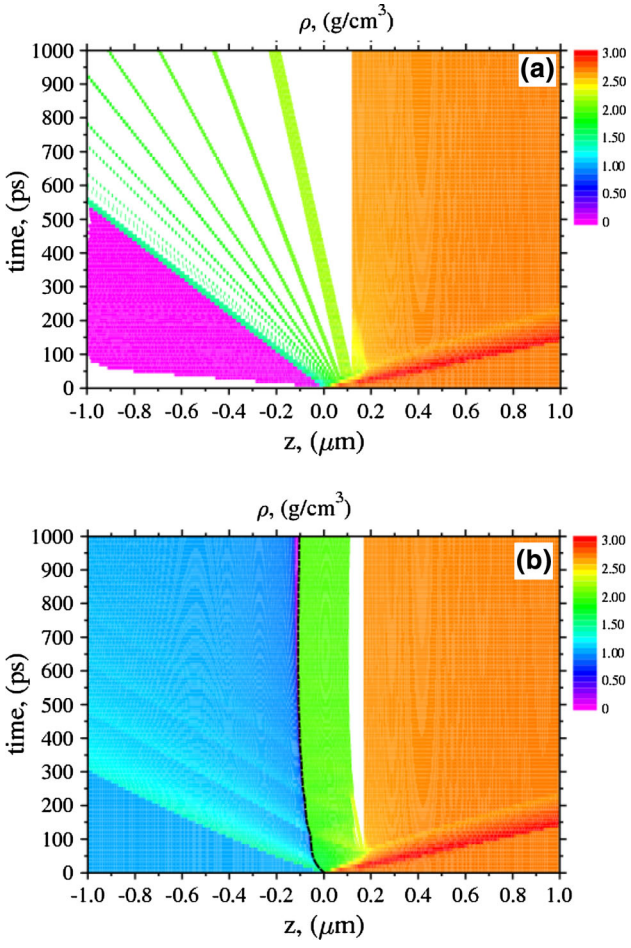

Fig. 1 Space–time diagram of density distribution. Al target ablation in vacuum—(**a**) and in water—(**b**) for $F = 1$ J/cm^2. *Dashed* (*black*) curve is the aluminum–water interface

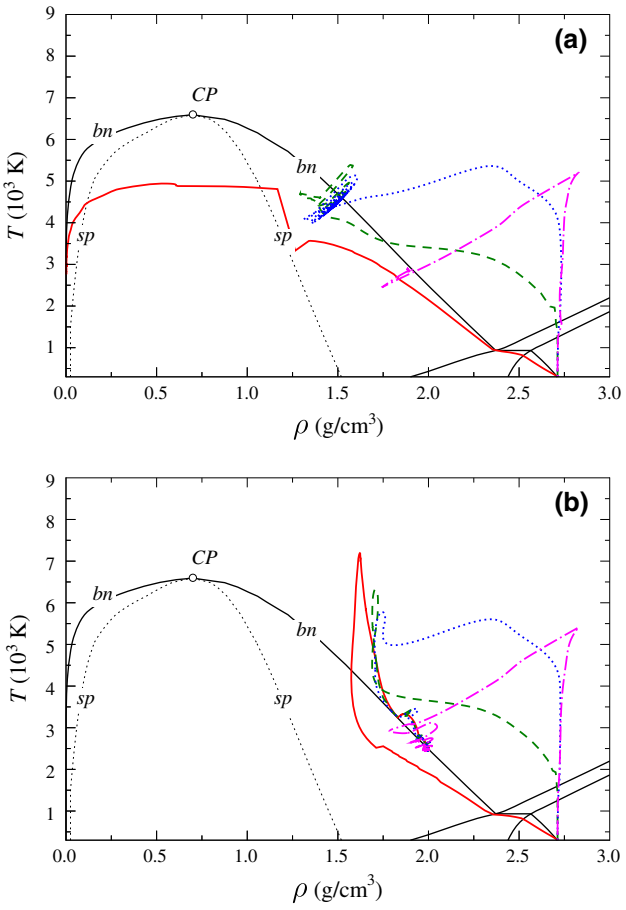

Fig. 2 Phase diagram of Al and thermodynamic trajectories of 1 nm (*solid red curve*), 5 nm (*dashed green curve*), 10 nm (*dotted blue curve*) and 50 nm (*dash-and-dot purple curve*) layers for Al target ablation in vacuum—(**a**) and in water—(**b**) for $F = 1$ J/cm^2. *CP* is the critical point, *bn* is binodal, *sp* is spinodal

aluminum target is located at $z \geq 0$ and vacuum or water is at $z < 0$.

In Fig. 1, we compare the ablation dynamics in vacuum and in water for laser fluence $F = 1$ J/cm^2. Laser fluence is calculated as follows $F = I_L \tau_L \sqrt{\pi / \ln(16)}$. As one can see, LA in vacuum results in the formation of thin layers of thicknesses from 10 to 50 nm already by time of 100 ps. In addition, a small region of a rarefied material is observed in front of the plume. Because acoustic impedance of water (ρc_s) is comparable in magnitude with that of aluminum, we observe the fast deceleration of the ablated material, see Fig. 1b. The acoustic oscillations in the detached layer then result in the formation of a set of waves in water. Furthermore, shock waves are formed in aluminum ($D \approx 6.7$ km/s) and water ($D \approx 3.3$ km/s), where D is the shock speed. The ablated layer is localized in the vicinity of the target surface in a distance shorter than 100 nm. In this layer of the molten aluminum, temperature reaches about 3,000 K and density is around 2 g/cm^3, see final parts of the trajectories in Fig. 2b. On the contrary, the temperature of the layers ablated in vacuum ranges from $\approx$5,000 K for 5 and 10 nm depths to $\approx$3,000 K for 50 nm depth, see the corresponding trajectories in Fig. 2a. Thus, primary NPs are expected to be smaller in the case of LA in vacuum.

For higher fluences, the ablation dynamics changes. First, a region of low-density target material is observed in the case of LA in vacuum, which corresponds to the liquid–gas mixture. In addition, the metastable liquid material is fragmented into a set of nanolayers. The size of these nanolayers varies here from several nanometers to hundreds of nanometers, see Fig. 3a.

Figure 4a shows the thermodynamic trajectories corresponding to the layers with the initial depths below the target surface of 1, 5, 10 and 50 nm. The presented results demonstrate a fast rarefaction of the target material, which undergoes transformation along supercritical and near-critical paths. Here, two basic mechanisms of NP creation are observed: (1) phase explosion in the vicinity of the critical point (CP); and (2) mechanical fragmentation of metastable liquid phase on rarefaction.

A strong confinement of the ablated plume is observed in the presence of water when fragmentation does not occur, Fig. 3b. The second temperature increase along 1, 5,

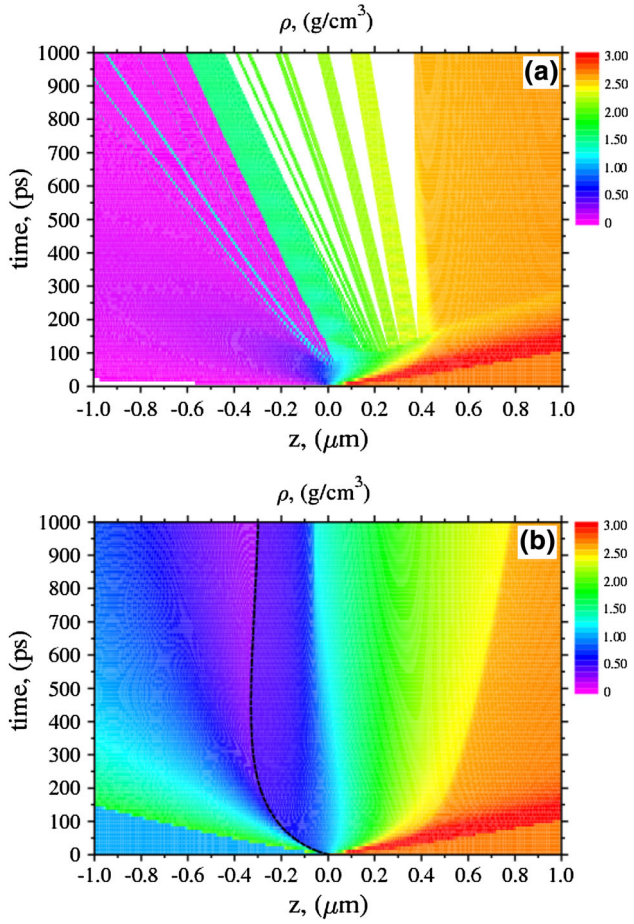

Fig. 3 The same as in Fig. 1 but for $F = 5$ J/cm^2

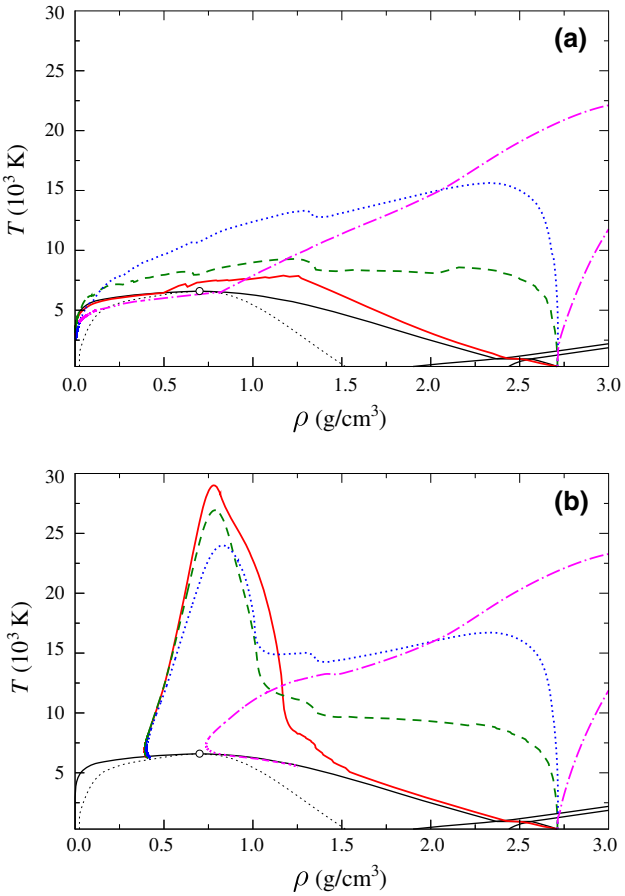

Fig. 4 The same as in Fig. 2 but for $F = 5$ J/cm^2

10 nm trajectories (Fig. 4b) takes place by the delay of $t \approx 4$ ps. This effect is caused by the confinement of the heat affected zone and electron–ion thermal equilibration. This, in turn, results in the increase in pressure at the water–aluminum interface resulting in the deceleration of the rarefaction process. For this reason, a thick molten layer is formed and reaches ≈ 1 μm by time of 1 ns. At that time, trajectories corresponding to the initial depths of 1, 5, 10 nm reach the metastable supersaturated gas phase and we expect a further decay of this state into a liquid–gas mixture. At the same time, the 50 nm trajectory (dash-and-dot purple curve) turns back and follows the binodal line, see Fig. 4b. Thus, only a thin layer of about 50 nm thickness is ablated (transformed into liquid–gas mixture) by 1 ns in the presence of water. For LA in vacuum, the corresponding depth is ≈ 300 nm under similar laser irradiations.

4 Conclusions

In conclusion, we have developed a two-temperature hydrodynamic model for simulation of aluminum target ablation in water. The numerical model describes laser energy absorption, thermal conduction, electron–ion coupling, shock and rarefaction wave propagation. For the description of thermodynamic properties of aluminum we add a thermodynamically complete multi-phase equation of state with stable and metastable phases.

A series of numerical calculation shows that NPs appear due to the liquid layer ejection and fragmentation. The regime of mechanical fragmentation of melted target layers is observed when the corresponding trajectories enter into the metastable region of the phase diagram. For higher laser intensities, the near-critical and supercritical trajectories appear and liquid–gas mixture is formed in the ablation plume. In the presence of an ambient liquid, LA is highly suppressed and the corresponding ablation threshold is much larger than that in vacuum. In this case, ablated layers are located closer to the target and are backscattered resulting in formation of a deep molten region on the surface of the target. Ablation of this layer at later delays leads to the additional NP formation.

We note, finally, that more detailed three-dimensional calculations should be performed to study longer time evolution of NPs. The developing of such a model is underway.

Acknowledgments The research was sponsored by France–Russia collaboration project PICS 6106, and by the Russian Foundation for Basic Research (Project Nos. 13-08-01179 and 13-02-91057-CNRS). We are also grateful to the CINES of France for the computer support under the project number c2013085015.

References

1. T. Makimura, Y. Kunii, K. Murakami, Jpn. J. Appl. Phys. **35**(Part1, No. 9A), 4780 (1996)
2. D.B. Geohegan, A.A. Puretzky, G. Duscher, S.J. Pennycook, Appl. Phys. Lett. **72**(23), 2987 (1998)
3. O. Albert, S. Roger, Y. Glinec, J. Loulergue, J. Etchepare, C. Boulmer-Leborgne, J. Perrire, E. Millon, Appl. Phys. A **76**(3), 319 (2003)
4. L.V. Zhigilei, B.J. Garrison, J. Appl. Phys. **88**(3), 1281 (2000)
5. M.E. Povarnitsyn, T.E. Itina, M. Sentis, P.R. Levashov, K.V. Khishchenko Phys. Rev. B **75**:235414 (2007)
6. A. Bulgakov, I. Ozerov, W. Marine, Appl. Phys. A **79**(4-6), 1591 (2004)
7. S. Amoruso, R. Bruzzese, N. Spinelli, R. Velotta, M. Vitiello, X. Wang Europhys. Lett. **67**(3), 404 (2004)
8. J. Freeman, S. Harilal, P. Diwakar, B. Verhoff, A. Hassanein Spectrochimica Acta Part B **87**(0), 43 (2013)
9. S. Amoruso, R. Bruzzese, M. Vitiello, N.N. Nedialkov, P.A. Atanasov, J. Appl. Phys. **98**(4), 044907 (2005)
10. A.V. Bulgakov, N.M. Bulgakova, J. Phys. D **28**(8), 1710 (1995)
11. Y.B. Zel'dovich, Y.P. Raizer, *Physics of Shock Waves and High-Temperature Hydrodynamic Phenomena. Dover Books on Physics* (Dover Publications, 2002)
12. B.S. Lukyanchuk, W. Marine, S.I. Anisimov Laser Phys. **8**(1), 291 (1998)
13. T. Ohkubo, M. Kuwata, B. Lukyanchuk, T. Yabe Appl. Phys. A **77**(2), 271 (2003)
14. F. Mafuné, J.Y. Kohno, Y. Takeda, T. Kondow, J. Phys. Chem. B **107**(46), 12589 (2003)
15. A.V. Simakin, E.N. Lubnin, G.A. Shafeev, Quant. Electron. **30**(3), 263 (2000)
16. J.P. Sylvestre, A.V. Kabashin, E. Sacher, M. Meunier Appl. Phys. A **80**, 753 (2005)
17. S. Ibrahimkutty, P. Wagener, A. Menzel, A. Plech, S. Barcikowski, Appl. Phys. Lett. **101**(10), 103104 (2012)
18. A. Vogel, V. Venugopalan, Chem. Rev. **103**(2), 577 (2003)
19. R. Fabbro, P. Peyre, L. Berthe, X. Scherpereel, J. Las. Appl. **10**, 265 (1998)
20. L. Berthe, R. Fabbro, P. Peyre, L. Tollier, E. Bartnicki, J. Appl. Phys. **82**(6), 2826 (1997)
21. E. Stratakis, M. Barberoglou, C. Fotakis, G. Viau, C. Garcia, G.A. Shafeev Opt. Expr. **17**(15), 12650 (2009)
22. A.V. Kabashin, M. Meunier, J. Appl. Phys. **94**(12), 7941 (2003)
23. A. Menéndez-Manjón, P. Wagener, S. Barcikowski, J. Phys. Chem. C **115**(12), 5108 (2011)
24. M.E. Povarnitsyn, T.E. Itina, P.R. Levashov, K.V. Khishchenko, Appl. Surf. Sci. **253**(15), 6343 (2007)
25. M.E. Povarnitsyn, T.E. Itina, P.R. Levashov, K.V. Khishchenko, Phys. Chem. Chem. Phys. **15**, 3108 (2013)
26. M.E. Povarnitsyn, N.E. Andreev, P.R. Levashov, K.V. Khishchenko, O.N. Rosmej, Phys. Plasm. **19**(2), 023110 (2012)
27. M.E. Povarnitsyn, N.E. Andreev, E.M. Apfelbaum, T.E. Itina, K.V. Khishchenko, O.F. Kostenko, P.R. Levashov, M.E. Veysman, Appl. Surf. Sci. **258**(23), 9480 (2012)